ChemComm

COMMUNICATION

View Article Online
View Journal | View Issue

Cite this: *Chem. Commun.*, 2023, **59**, 2644

Received 24th November 2022,
Accepted 3rd February 2023

DOI: 10.1039/d2cc06376j

rsc.li/chemcomm

Distorted B/O-containing nanographenes with tunable optical properties†

Jiaxiang Guo,[a] Tianyu Zhang,[a] Zeyi Li,[a] Kaiqi Ye,[a] Yue Wang[a] and Chuandong Dou*[ab]

We report the synthesis of two B/O-containing nanographenes, which feature the fusion of three or six planar B/O-heterocycles onto one hexa-peri-hexabenzocoronene π-framework. Incorporation of the B/O-heterocycles not only leads to distorted geometries, but also modulates the electronic structures and results in gradually red-shifted absorptions and fluorescence.

Polycyclic aromatic hydrocarbons (PAHs) and synthetic nanographenes (NGs) have received great attention owing to their intriguing topological structures and widespread applications in electronics, spintronics and bioimaging.[1] Incorporating heterocycles is an efficient strategy not only to construct diverse structures but also to modulate the electronic nature and properties.[2] Indeed, a variety of heterocyclic NGs containing B, N, O, P or S atoms have been dramatically developed, which display interesting optical and electronic properties.[3] Moreover, nonplanar or contorted PAHs possess unusual conformations, molecular stacking modes and functions, such as disturbed π–π stacking, which is of importance for supramolecular assembly or semiconductors employing intermolecular electronic interactions.[4] Therefore, the construction of distorted heterocyclic NGs has emerged as an attractive research topic from both the synthetic chemistry and materials science point of view.

Hexa-peri-hexabenzocoronene (**HBC**), owning a planar configuration with a diameter of over 1 nm, is one of the most representative NG molecules.[5] Introducing non-hexagonal rings or defective edges into the **HBC** scaffold has afforded various structure-extended NGs with amazing nonplanar topologies.[6] For instance, chiral NGs and even graphene nanoribbons containing single/multiple helical regions have been developed as a novel series of circularly polarized luminescence emitters.[6b,d] Severely contorted or negatively curved NGs based on **HBC** have also been synthesized, which display attractive electronic structures and molecular assembly behaviours.[6e] However, **HBC**-based heterocyclic NGs are rarely explored, though incorporation of heterocycles onto **HBC** may modulate its molecular conformation and alter its physical properties. Typically, hexa-peri-hexabenzoborazinocoronene bearing an internal B_3N_3 ring, prepared using solution-phase and on-surface synthetic chemistry, exhibits a larger energy gap in comparison to all-carbon **HBC**.[7]

Working in a research area of heterocyclic analogs of polycyclic hydrocarbons, we recently reported rapid π-extension of conjugated organoboranes as an effective methodology for creating nanoscale B-doped PAHs.[8] One example is a new kind of pristine B-doped molecular ribbon, which not only has contorted geometries with up to 2.2 nm in length but also displays unexpected photochromism properties and charge-transporting properties. In this study, we disclose hybridization of **HBC** and B/O-heterocycles to design distorted heterocyclic NGs (Fig. 1). Two B/O-containing NGs (**HBC-3BO** and **HBC-6BO**) that feature the fusion of three or six planar B/O-heterocycles (PBO) onto one **HBC** π-framework were synthesized. These B/O-heterocycles

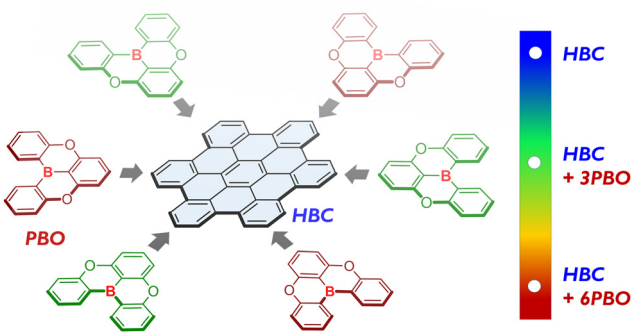

Fig. 1 Molecular design of **HBC-3BO** and **HBC-6BO**.

[a] *State Key Laboratory of Supramolecular Structure and Materials, College of Chemistry, Jilin University, Changchun 130012, P. R. China. E-mail: chuandong@jlu.edu.cn*
[b] *Jiangsu Engineering Laboratory of Novel Functional Polymeric Materials, Soochow University, Suzhou, 215123, P. R. China*

† Electronic supplementary information (ESI) available: Experimental details, thermal and photophysical properties, single-crystal analysis, and theoretical calculations. CCDC 2221600. For ESI and crystallographic data in CIF or other electronic format see DOI: https://doi.org/10.1039/d2cc06376j

produce distorted configurations owing to the formation of multiple helical regions, and moreover, modulate their electronic structures and thus optical properties, as revealed by detailed theoretical and experimental studies.

Scheme 1 shows the synthesis of these two B/O-containing NGs, in which the B/O-heterocycle was first reported by Hatakeyama *et al.* and was recently employed to develop B-containing organic diradicaloids.[9,10] A cyclotrimerization reaction of alkyne derivative **1** with $Co_2(CO)_8$ as the catalyst afforded key precursor **2** in 25% yield. Intramolecular cyclodehydrogenation (*i.e.*, the Scholl reaction) of **2** with an excess of $FeCl_3$ produced **HBC-3BO** in 75% yield as an orange-yellow solid. For **HBC-6BO**, the branched alkyl chains were used to enhance its solubility. The cyclotrimerization reaction was similarly performed on **3** to form **4**. In the cyclodehydrogenation reaction of **4**, 2,3-dichloro-5,6-dicyano-1,4-benzoquinone (DDQ) and trifluoromethanesulfonic acid (TfOH) were used to efficiently generate **HBC-6BO** as a pink solid in 45% yield, whereas $FeCl_3$ led to a mixture of fully and partially fused products.[11] These two B/O-containing NGs have good stability and can be purified by silica gel column chromatography under ambient conditions.

The structures of **HBC-3BO** and **HBC-6BO** were confirmed by NMR spectroscopy and high-resolution mass spectrometry (HRMS). The HRMS spectra exhibit intense signals at m/z = 1602.8214 for **HBC-3BO** and 3020.8801 for **HBC-6BO** along with clear isotopic distributions, which agree well with the calculated molecular mass and simulated patterns of their molecular formula of $C_{114}H_{105}B_3O_6$ and $C_{210}H_{240}B_6O_{12}$, respectively (Scheme 1). The well-resolved ^{1}H NMR spectra of **HBC-3BO** and **HBC-6BO** were recorded in C_6D_6 and $C_2D_2Cl_4$ at room temperature, respectively. It is notable that **HBC-3BO** and **HBC-6BO** exhibit only four and three different signals in the aromatic region, respectively, which are clearly assigned to the protons. These simple proton signals also demonstrate their highly symmetric structures in solution.

Single crystals of **HBC-3BO** suitable for X-ray structural analysis were obtained by slow diffusion of CH_3OH into its $CHCl_3$ solution. Twenty-five hexagons are fused together to form a large skeleton that features the fusion of three PBO moieties onto **HBC** with the formation of six cove regions. Thus, a distorted geometry with the (*P, P, M, M, M*, and *M*) conformation is obtained due to the steric repulsion in the cove regions (Fig. 2).

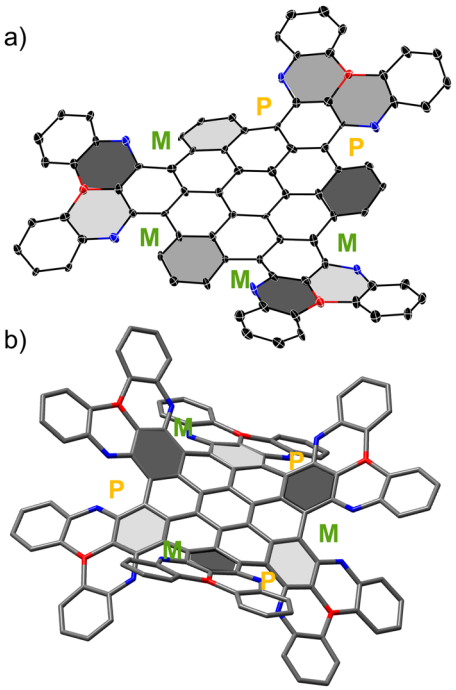

Fig. 2 (a) Single-crystal structure of **HBC-3BO** (50% probability for thermal ellipsoids). (b) Optimized structure of **HBC-6BO′**, calculated at the B3LYP/6-311G(d) level. The alkyl groups were omitted in **HBC-3BO** for clarity and in **HBC-6BO′** for simplified calculations.

Torsional angles of these helical regions range from 6.5(17)° to 23.4(15)°, indicative of the moderately contorted topology of the framework and facile conversion from one conformation to others (Fig. S1, ESI†). Despite the distorted configuration, **HBC-3BO** shows a slipped face-to-face packing mode, accompanied by a large π–π overlap and a small π–π stacking distance of 3.35 Å (Fig. S3, ESI†). For **HBC-6BO**, we did not obtain its single crystals due to the flexible branched alkyl chains. We thus optimized its model compound **HBC-6BO′** for structural analysis. According to the density functional theory (DFT) calculations (B3LYP/6-311G(d) level), there are fourteen possible stereoisomers caused by B/O-containing [5]-helicenes, and notably, the waggling (*P, M, P, M, P*, and *M*) conformation has

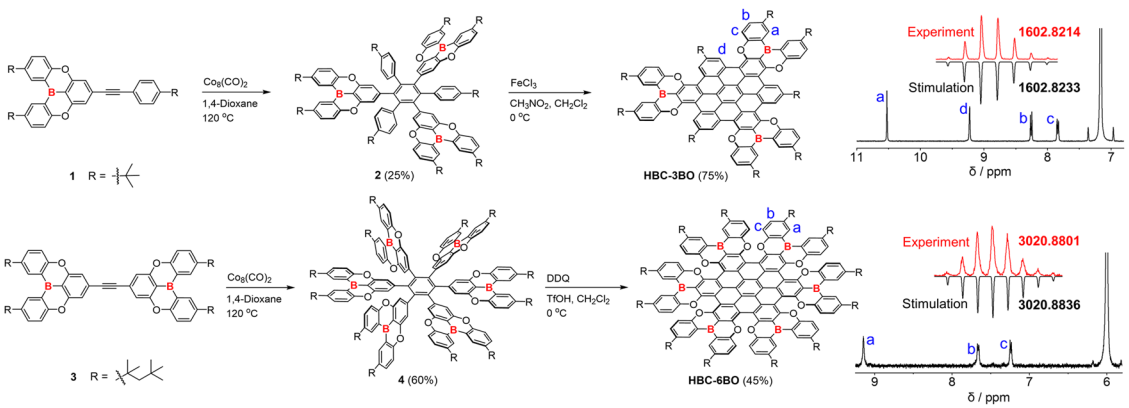

Scheme 1 Synthesis of **HBC-3BO** and **HBC-6BO**. Insets are their HRMS and ^{1}H NMR spectra.

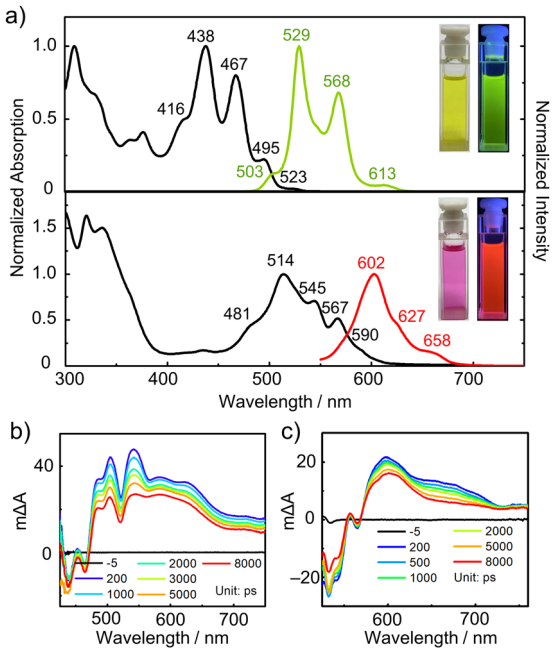

Fig. 3 (a) The UV/Vis absorption and fluorescence spectra of **HBC-3BO** and **HBC-6BO** in toluene (1×10^{-5} M^{-1}). Insets are the photographs of their toluene solutions under room light (left) and irradiation with UV light (right). The transient absorption (TA) spectra of (b) **HBC-3BO** and (c) **HBC-6BO** in toluene.

the lowest total energy (Fig. S8, ESI†). Six PBO moieties adopt an "up-down" arrangement with an enhanced torsional angle of 38.3°.[12] In addition, the B/O-containing [5]-helicene, as the structural fragment of **HBC-6BO′**, has a theoretically estimated activation energy ($\Delta G^{\ddagger}$) of 20.8 kcal mol^{-1} for conformational conversion, which is slightly smaller than that (24.1 kcal mol^{-1}) of all-carbon [5]-helicene (Fig. S9, ESI†). These relatively small $\Delta G^{\ddagger}$ values suggest that the conformations of **HBC-6BO** may show facile interconversion in solution, which is consistent with the ^{1}H NMR result.

The optical properties of these B/O-containing NGs are greatly influenced by the B/O-heterocycles. As shown in Fig. 3, **HBC-3BO** and **HBC-6BO** in toluene display yellow and purple colors, respectively, and well-resolved vibronic absorption spectra. While **HBC-3BO** exhibits a main adsorption band with maxima (λ_{abs}) at 438/467 nm along with shoulder peaks at 416/495/523 nm, **HBC-6BO** shows a absorption maxima at 514/545 nm and shoulder peaks at 481/567/590 nm. According to the onset adsorption, the optical band gap (E_g^{opt}) values are calculated to be 2.44 eV for **HBC-3BO** and 2.10 eV for **HBC-6BO**. Strong green and red fluorescence is observed for their toluene solutions, respectively. In the fluorescence spectra, **HBC-3BO** has maximum emission peaks (λ_{em}) at 529/568 nm and weak tails at 503/613 nm, whereas **HBC-6BO** exhibits one main emission band at 602 nm along with shoulder peaks at 627/658 nm. The fluorescence quantum yields and lifetimes are determined to be 18% and 4.6/21.4 ns for **HBC-3BO** and 20% and 5.7/10.2 ns for **HBC-6BO** (Fig. S6, ESI†). In comparison to **HBC** containing six *t*-butyl groups (*t*Bu-**HBC**), **HBC-3BO** and **HBC-6BO** display significantly red-shifted absorption bands by 78 and 154 nm, respectively (Table S1, ESI†).[13] Moreover, from *t*Bu-**HBC** to **HBC-3BO** and **HBC-6BO**, the main emission bands are bathochromically shifted by 36 and 109 nm, respectively, along with increased fluorescence quantum yields. The remarkably red-shifted absorption and emissions for B/O-containing NGs can be attributed to the great electronic effects of B/O-heterocycles (*vide infra*).

The excited-state dynamics were investigated by performing transient absorption (TA) spectroscopy measurements on **HBC-3BO** and **HBC-6BO** in toluene. As shown in the TA spectra (Fig. 3b and c), broad excited-state absorption (ESA) bands are observed at 480–740 nm for **HBC-3BO** and 560–740 nm for **HBC-6BO**. The ground-state bleach (GSB) signals appear at 425–480 nm for **HBC-3BO** and at 520–550 nm for **HBC-6BO**, which match well with their low-energy absorption peaks of the steady-state absorption spectra, respectively. While the stimulated emission (SE) signal is observed at 528 nm as a negative and overwhelming bump for **HBC-3BO**, such a signal of **HBC-6BO** cannot be detected probably because of the complete overwhelming by its ESA band.[14] The excited-state lifetimes (τ) are determined to be 17.6 ps and 21.8 ns for **HBC-3BO** and 61.0 ps and 24.8 ns for **HBC-6BO**, respectively, based on the fitting of the decay profiles by a two-exponential function (Fig. S7, ESI†). These short and relatively long lifetimes can be ascribed to internal conversion and radiative relaxation processes, respectively.[15]

To elucidate the effects of the B/O-heterocycles on the electronic structure of **HBC**, we performed density functional theory (DFT) calculations at the B3LYP/6-311G(d) level of theory on the model compounds **HBC**, **HBC-3BO′** and **HBC-6BO'**. Their Kohn–Sham molecular orbitals from HOMO−2 to LUMO+1 are shown in Fig. 4. While the LUMO and LUMO+1 as well as the HOMO and HOMO−1 in **HBC** are well delocalized on the π-skeleton and almost identical in energy, the HOMO−2 with a lower energy is localized on its peripheral region. From **HBC** to **HBC-3BO′**, the distributions of the HOMO, HOMO−1 and HOMO−2 are slightly modulated only with elevated energies by 0.3–0.6 eV. In contrast, the LUMO and LUMO+1 are lowered by 0.3 eV in energy along with their distributions

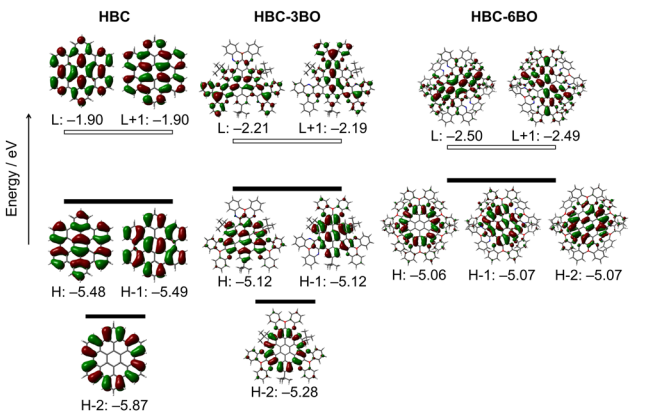

Fig. 4 Kohn–Sham molecular orbitals of **HBC**, **HBC-3BO** and **HBC-6BO**.

extending to the B/O-heterocycles, in which the vacant p orbital of the B atom contributes significantly. From **HBC-3BO′** to **HBC-6BO′**, the LUMO and LUMO+1 are further decreased by 0.3 eV in energy accompanied by the perturbed distributions, and the HOMO, HOMO−1 and HOMO−2 have almost identical energy due to the obviously increased energy by 0.22 eV for the HOMO−2. As a result, from **HBC** to **HBC-3BO′** and **HBC-6BO′**, the energy gap is gradually decreased. These changes indicate that incorporation of the B/O-heterocycles onto **HBC** significantly impacts its electronic structure, especially the electronic energy levels and distributions of molecular orbitals, which can be attributed to the synergetic effects of the electron-accepting B atoms and electron-donating O atoms in the B/O-heterocycles.

To gain insight into the absorption properties of these B/O-containing NGs, we conducted time-dependent DFT (TD-DFT) calculations on **HBC-3BO′** and **HBC-6BO′**. The absorption band at 438/467 nm of **HBC-3BO** is assignable to the allowed electronic transitions of $S_0 \rightarrow S_3$, $S_0 \rightarrow S_4$, $S_0 \rightarrow S_5$ and $S_0 \rightarrow S_6$ (Fig. S10, ESI†). For **HBC-6BO**, the absorbance observed around 514/545 nm is assigned to the transitions of $S_0 \rightarrow S_5$ and $S_0 \rightarrow S_6$ (Fig. S11, ESI†). The theoretical spectra including energies, wavelengths and oscillator strengths agree well with the experimental results. It is noteworthy that their LUMO and LUMO+1 are all involved in these electronic transitions. It is thus suggested that the B atom in the B/O-heterocycle plays an important role in producing the red-shifted absorption of B/O-containing NGs.

In summary, we synthesized two B/O-containing nanographenes, **HBC-3BO** and **HBC-6BO**, which feature the fusion of three or six planar B/O-heterocycles onto one **HBC** π-framework. Incorporation of the B/O-heterocycles leads to multiple helical regions, thus producing their obviously distorted geometries. Moreover, these B/O-heterocycles greatly impact on the electronic structure of **HBC** and thus give rise to the gradually red-shifted absorptions and fluorescence of B/O-containing NGs, for instance, the maximum emission peak is 493 nm for *t*Bu-**HBC**, 529 nm for **HBC-3BO** and 602 nm for **HBC-6BO**. This study thus proves that hybridization of B/O-heterocycles and π-systems is a promising strategy toward the construction of distorted heterocyclic NGs together with modulations of the electronic structures and properties, which may be applied to the production of sophisticated π materials.

Support has been provided by the Jilin Scientific and Technological Development Program (No. 20220101054JC) and the National Natural Science Foundation of China (No. 22175074). We thank the crystallography reviewer for his kind help on the single-crystal data.

Conflicts of interest

There are no conflicts to declare.

Notes and references

1 (*a*) A. Narita, X.-Y. Wang, X. Feng and K. Müllen, *Chem. Soc. Rev.*, 2015, **44**, 6616–6643; (*b*) M. Grzybowski, B. Sadowski, H. Butenschön and D. T. Gryko, *Angew. Chem., Int. Ed.*, 2020, **59**, 2998–3027; (*c*) Y. Segawa, H. Ito and K. Itami, *Nat. Rev. Mater.*, 2016, **1**, 15002; (*d*) J. Liu and X. Feng, *Angew. Chem., Int. Ed.*, 2020, **59**, 23386–23401.

2 (*a*) M. Hirai, N. Tanaka, M. Sakai and S. Yamaguchi, *Chem. Rev.*, 2019, **119**, 8291–8331; (*b*) A. Borissov, Y. K. Maurya, L. Moshniaha, W.-S. Wong, M. Żyła-Karwowska and M. Stępień, *Chem. Rev.*, 2022, **122**, 565–788; (*c*) W. Jiang, Y. Li and Z. Wang, *Acc. Chem. Res.*, 2014, **47**, 3135–3147.

3 (*a*) S. R. Peurifoy, T. J. Sisto, F. Ng, M. L. Steigerwald, R. Chen and C. Nuckolls, *Chem. Rec.*, 2019, **19**, 1050–1061; (*b*) X.-Y. Wang, X. Yao, A. Narita and K. Müllen, *Acc. Chem. Res.*, 2019, **52**, 2491–2505; (*c*) E. von Grotthuss, A. John, T. Kaese and M. Wagner, *Asian J. Org. Chem.*, 2018, **7**, 37–53; (*d*) X. Yang, S. M. Elbert, F. Rominger and M. Mastalerz, *J. Am. Chem. Soc.*, 2022, **144**, 9883–9892; (*e*) S. Seifert, K. Shoyama, D. Schmidt and F. Würthner, *Angew. Chem., Int. Ed.*, 2016, **55**, 6390–6395.

4 (*a*) I. R. Márquez, S. Castro-Fernández, A. Millán and A. G. Campaña, *Chem. Commun.*, 2018, **54**, 6705–6718; (*b*) Chaolumen, I. A. Stepek, K. E. Yamada, H. Ito and K. Itami, *Angew. Chem., Int. Ed.*, 2021, **60**, 23508–23532; (*c*) R. K. Dubey, M. Melle-Franco and A. Mateo-Alonso, *J. Am. Chem. Soc.*, 2021, **143**, 6593–6600; (*d*) J. Liu, B.-W. Li, Y.-Z. Tan, A. Giannakopoulos, C. Sanchez-Sanchez, D. Beljonne, P. Ruffieux, R. Fasel, X. Feng and K. Müllen, *J. Am. Chem. Soc.*, 2015, **137**, 6097–6103; (*e*) Y. Tanaka, N. Fukui and H. Shinokubo, *Nat. Commun.*, 2020, **11**, 3873; (*f*) Y. Chen, C. Lin, Z. Luo, Z. Yin, H. Shi, Y. Zhu and J. Wang, *Angew. Chem., Int. Ed.*, 2021, **60**, 7796–7801; (*g*) W. Zeng, H. Phan, T. S. Herng, T. Y. Gopalakrishna, N. Aratani, Z. Zeng, H. Yamada, J. Ding and J. Wu, *Chem*, 2017, **2**, 81–92; (*h*) S. H. Pun and Q. Miao, *Acc. Chem. Res.*, 2018, **51**, 1630–1642.

5 J. Wu, W. Pisula and K. Müllen, *Chem. Rev.*, 2007, **107**, 718–747.

6 (*a*) Y. Zhang, S. H. Pun and Q. Miao, *Chem. Rev.*, 2022, **122**, 14554–14593; (*b*) C. Cruz, S. Castro-Fernández, E. Maçôas, A. Millán and A. Campaña, *Synlett*, 2019, 997–1002; (*c*) W.-S. Wong and M. Stępień, *Trends Chem.*, 2022, **4**, 573–576; (*d*) Y. Zhu, X. Guo, Y. Li and J. Wang, *J. Am. Chem. Soc.*, 2019, **141**, 5511–5517; (*e*) S. H. Pun, C. K. Chan, J. Luo, Z. Liu and Q. Miao, *Angew. Chem., Int. Ed.*, 2018, **57**, 1581–1586.

7 (*a*) M. Krieg, F. Reicherter, P. Haiss, M. Ströbele, K. Eichele, M.-J. Treanor, R. Schaub and H. F. Bettinger, *Angew. Chem., Int. Ed.*, 2015, **54**, 8284–8286; (*b*) J. Dosso, J. Tasseroul, F. Fasano, D. Marinelli, N. Biot, A. Fermi and D. Bonifazi, *Angew. Chem., Int. Ed.*, 2017, **56**, 4483–4487.

8 (*a*) W. Sun, J. Guo, Z. Fan, L. Yuan, K. Ye, C. Dou and Y. Wang, *Angew. Chem., Int. Ed.*, 2022, **61**, e2022092; (*b*) L. Yuan, J. Guo, Y. Yang, K. Ye, C. Dou and Y. Wang, *CCS Chem.*, 2022, DOI: 10.31635/ccschem.022.202101738.

9 H. Hirai, K. Nakajima, S. Nakatsuka, K. Shiren, J. Ni, S. Nomura, T. Ikuta and T. Hatakeyama, *Angew. Chem., Int. Ed.*, 2015, **54**, 13581–13585.

10 (*a*) J. Guo, Y. Yang, C. Dou and Y. Wang, *J. Am. Chem. Soc.*, 2021, **143**, 18272–18279; (*b*) X. Tian, J. Guo, W. Sun, L. Yuan, C. Dou and Y. Wang, *Chem. – Eur. J.*, 2022, **28**, e202200045.

11 (*a*) X. Yang, F. Rominger and M. Mastalerz, *Angew. Chem., Int. Ed.*, 2019, **58**, 17577–17582; (*b*) T. Dumslaff, Y. Gu, G. M. Paternò, Z. Qiu, A. Maghsoumi, M. Tommasini, X. Feng, F. Scotognella, A. Narita and K. Müllen, *Chem. Sci.*, 2020, **11**, 12816–12821.

12 (*a*) M. Żyła-Karwowska, H. Zhylitskaya, J. Cybińska, T. Lis, P. J. Chmielewski and M. Stępień, *Angew. Chem., Int. Ed.*, 2016, **55**, 14658–14662; (*b*) M. Navakouski, H. Zhylitskaya, P. J. Chmielewski, T. Lis, J. Cybińska and M. Stępień, *Angew. Chem., Int. Ed.*, 2019, **58**, 4929–4933.

13 J. M. Fernández-García, P. J. Evans, S. Medina Rivero, I. Fernández, D. García-Fresnadillo, J. Perles, J. Casado and N. Martín, *J. Am. Chem. Soc.*, 2018, **140**, 17188–17196.

14 T. Dumslaff, Y. Gu, G. M. Paternò, Z. Qiu, A. Maghsoumi, M. Tommasini, X. Feng, F. Scotognella, A. Narita and K. Müllen, *Chem. Sci.*, 2020, **11**, 12816–12821.

15 G. M. Paternò, Q. Chen, X.-Y. Wang, J. Liu, S. G. Motti, A. Petrozza, X. Feng, G. Lanzani, K. Müllen, A. Narita and F. Scotognella, *Angew. Chem., Int. Ed.*, 2017, **56**, 6753–6757.